International Journal of Thermal Sciences 137 (2019) 627–639

Contents lists available at ScienceDirect

International Journal of Thermal Sciences

journal homepage: www.elsevier.com/locate/ijts

Empirical correlations for mixed convection heat transfer through a fin array based on various orientations

Raad Z. Homod[a,*], Falah A. Abood[b], Sana M. Shrama[b], Ahmed K. Alshara[c]

[a] Department of Oil and Gas Engineering, Basra University for Oil and Gas, Iraq
[b] Department of Mechanical Engineering, Basrah University, Iraq
[c] Department of Civil Engineering, Messan University, Iraq

ARTICLE INFO

Keywords:
Mixed convection
Correlation
Channel orientation
Lateral inclination angle
Longitudinal inclination angle
Fin array

ABSTRACT

The transfer of heat by the fins is influenced by the change of the direction of the fins. This paper investigates study the effect of the direction of longitudinal fins on a three-dimensional convection heat transfer in a rectangular channel and also study the effect of the lateral and longitudinal inclination of the rectangular channel. The Grashof range from 5×10^8 to 10^9, Reynolds from 1000 to 2300 and Prandtl 0.71. The bottom surface of the channel is exposed to constant heat flux, while other walls are isolated. Two cases are investigated. In case one, measurements were conducted for a lateral inclination of the channel, with a range of $\alpha = 0^\circ$,30°,60°, and 90°. Case two studied the longitudinal inclination of the channel, with the lateral inclination angle fixed at $\alpha = 90^\circ$ and the longitudinal inclination angle $\Theta = 0^\circ$, 30°, 60°, and 70°. The dimensionless of fin height was Hf/H = 0.6, and the fin spacing was S/H = 0.17. The experimental results show that the coefficient of the heat transfer for lateral inclination ($\alpha = 0^\circ$) was greater than that for a sideways orientation ($\alpha = 90^\circ$). Additionally, the average coefficient of heat transfer for both the lateral and longitudinal inclination case is increased with the longitudinal inclination angle. The empirical equations are obtained based on the experimental results. These equations correlated the Nusselt number as a dependent variable of the orientations angles, Reynolds number, and the Grashof number, these equations are consistent with experimental results.

1. Introduction

Most engineering applications consume energy and associated with produce heat [1,2]. This heat production is usually an undesirable side effect that decreases the system performance, each engineering system is designed almost to operate within a specified range of temperatures [3]. Failure of a system occurs when these limits are surpassed by overheating [4]. Therefore, many engineering systems try to avoid this overheating problem as much as possible by using different methods for dissipating heat away from the system to surrounding areas [5]. The energy of heat is released in several ways; systems that operate give energy in the form of heat, chemical reactions release latent energy such as heat, electrons that flow through materials that generate heat, pressure gases generate heat, and radiation matter creates heat [6].

In the design and construction of different types of energy (heat) transfer systems, different devices, such as cylinders, rods, and plates, are used to achieve heat flow between the source and the sink. These structures provide surfaces for absorption or rejection of heat and are defined as main surfaces [7].

To increasing heat transfer from surfaces are usually used fins when it is not possible to increase the rate of heat transfer, either by increasing the coefficient of heat transfer on the surface or by increasing the difference of temperature between the surface and the fluid [8]. In the system of electronic thermal management, heat sinks are usually attached to the tops of the electronic package to enhance heat dissipation and control the junction temperatures of these packages [9]. The main desired goal of the design of heat sink is a substantial enhancement of the heat transfer by convection with minimal increases in the pressure drop of streamwise. The rectangular fins are widely used to increase the rate of heat dissipation of the systems because they are simple and inexpensive to manufacture. The transfer of convective heat within a channel containing fins was studied by many researchers [10–14].

The convection heat transfer in rectangular enclosures is studied numerically by Lakhal et al. [10] with perfectly attached fins to the hot wall. The effective parameters for this problem are the enclosures aspect ratio is $2.5 \leq AR \leq \infty$, the Rayleigh number is $10^2 \leq Ra \leq 2 \times 10^5$, the dimensionless partitions lengths are $0 \leq B \leq 1$, the angle

* Corresponding author.
E-mail address: raadahmood@yahoo.com (R.Z. Homod).

https://doi.org/10.1016/j.ijthermalsci.2018.12.012
Received 5 May 2017; Received in revised form 9 December 2018; Accepted 10 December 2018

Nomenclature

A_b	surface area of plate, m^2
A_c	area of channel cross sectional, m^2
D_h	hydraulic diameter of the channel, m
g	gravitational force, m/s^2
h_{av}	the average of heat transfer coefficient, W/mK
H	height of the channel, in
H_f	height of the fin, m
I	current, A
K	conductivity, W/mK
L	length, m
L_f	length of the fin, m
Nu_{av}	average Nusselt number
P	perimeter, m
q_{con}	convection heat flux, W/m^2
Q_{conv}	convection heat transfer rate, W
Q_{cond}	conduction heat transfer rate, W
Q_{rad}	the rate of radiation heat transfer, W
Q_{total}	total dissipation of the power, W
Ra	Rayleigh number
Re	Reynolds number
T	temperature, ˚C
T_b	bulk mean temperature, ˚C
T_{in}	inlet emperature of the ah,˚C
T_w	average temperature of the aluminium plate surface, ˚C
W_{in}	mean longitudinal velocity, m/s
V	voltage, V
W	width, m

Greek symbols

α	diffusivity, m^2/s
α	lateral inclination angle
Θ	longitudinal inclination angle
β	coefficient or thermal expansion, 1/K
ε	emissivity
μ	dynamic viscosity, kg/ms
ν	kinematic viscosity, m^2/s
σ	Stefan–Boltzmann constant W/m^2K^4

Subscripts

f	fin
in	inlet
w	wall

of inclination $0 \leq \Theta \leq 60$ and Pr = 0.72. The results show that at low Rayleigh numbers, the heat transfer system is dominated by conduction [11]. Huang et al. [12] they studied experimentally the heat transfer by natural convection from square pin fin heat sinks subjected to the orientation effect. A seven square pin fin heat sinks and a flat plate with different arrangements were tested in a controlled environment. The results show that the downward facing orientation gives the lowest coefficient of heat transfer. Therefore, the coefficients of heat transfer for sideways and upward orientations are of comparable magnitude. The test was carried on a trapezoidal fin heat sink with various orientations under a controlled environment.

Experiments on the heat transfer by natural convection from trapezoidal fin array heat sinks subjected to the orientation effect were carried out by Al-Azawi [15]. A trapezoidal fin heat sink with various orientations was tested in a controlled environment. The author pointed out that the sideways horizontal fin gave the lowest coefficient of heat transfer, while the sideways vertical fin yield the best performance of natural cooling. Of these experiments, Nu was defined as a function of Ra at Pr = 0.7 for each direction, with Ra between 1400 and 3900. The results showed that the heat transfer coefficients for sideways vertical fins higher than those of upward fins by 12%, while higher than the downward fins by 26% and by120% than of sideways horizontal fins. Moreover, Naidu et al. [16] They studied theoretically and experimentally the heat transfer problem by natural convection from a fins array to find the effect of the base inclination of fins array on the rate of heat transfer. A numerical model was developed by taking the can, formed from a horizontal base and between two adjacent vertical fins. All the governing equations for a fluid, together with the equations of heat conduction in each fin, were resolved using the method of alternate Direct Implicit. The experimental studies were carried out for five different longitudinal inclinations, including 0˚, 30˚, 45˚, 60˚, and 90˚. In addition, the natural convection heat transfer from a heat sink with narrow plate-fins and a parallel arrangement mounted on an inclined base is experimentally investigated by Walunj and Palande [17]. The rectangular base was tilted at an angle of 0˚, 10˚, 20˚, 45˚, 70˚, 80˚, and 90˚ while the fins were facing upwards. The results showed that the rate of convection heat transfer decreases by increasing fin length and increases by increasing fin height. Furthermore, the heat transfer is increased by convection with an increase in the aspect ratio, but this behavior was different for different tilt angles. In addition, Ahmed [18] The CFD software Ansys/Fluent was used to study the effect of the longitudinal inclination angle for a plate heat shield for different Reynold numbers and different of fin heights on the hydraulic and thermal performance of heat sink. The study showed that a variation of the longitudinal inclination angle caused a complicated and substantial flow field variation in space both upstream and downstream near a heat sink. In addition, experimental simulations are performed by Maughan and Incropera [19], to investigate the effects of longitudinal fins on laminar mixed convection in airflow between parallel plates, with isothermally heated for the bottom plate while the upper plate is cooled with constant temperature. The results were that no secondary flow was evident for conditions of fully developed on the without fins plate until the Rayleigh number exceeded the critical value 1708. Beyond that, longitudinal vortices were formed and persisted in decaying into turbulence at Ra = 20,000. Dogan and Sivrioglu [20] and Taji et al. [21] A similar experimental study was performed on heat transfer by mixed convection from longitudinally arranged fins within a horizontal duct to find highest heat transfer and find the optimal value for the ratio of the fin height to the spacing between fins. An experimental study was carried out to find the effect of spacing between fins and fin height as well as the heat flux on combined convection heat transfer from a fins array heated from the bottom inside a horizontal channel. Results showed that the optimum spacing of the fins that gave the maximum heat transfer is S = 8–9 mm and that the optimal spacing depends on Ra*. Moreover, Yang et al. [22] Das et al. [23] They studied combined convection heat transfer in an inclined parallel plates channel with transverse fins attached to the bottom wall of the channel. Their results indicated that, for Gr/Re = 10, the optimum aspect ratio increased with an increase in the longitudinal angle of inclination, while the orientation effect on the optimum aspect ratio was not pronounced for Gr/Re < 1.

Only a few information can be found in the available literature on experiments of the heat transfer by mixed convection from a fins array fitted in a horizontal duct. However, some transient convection heat transfer studies by implemented within ducts with longitudinal angles, but none of the previous studies represented the effect of the lateral tilt angles of the channel on the heat transfer process. The current study experimentally reports the effect of longitudinal inclination angles and lateral tilt angles of the channel on a laminar mixed convection heat transfer in three dimensions from a rectangular fins array attached to

the heated wall of the duct. In order to achieve the highest heat transfer, the lateral tilt angles and longitudinal inclination angles are considered to optimize them for a condition of constant heat flux [24].

2. Experimental apparatus

An experimental setup description is presented with the experimental procedure discussion. A wind tunnel is built with a longitudinal fin array to investigate the performance of the tested fin array. A schematic drawing is shown in Fig. 1. The orientations of the experimental setup selected here are shown in Fig. 2, which include a longitudinal and lateral inclination.

2.1. Open air stream

The induced draft fan was used to drive the cooling medium (air), which was controlled by a valve. The wind tunnel was made from galvanized iron and contains a damping chamber made of a 20 × 30 × 50 cm and 20 cm long inlet nozzle. The outlet nozzle is 30 cm long. The fan is induced the air then enters the damping chamber, to suppress the turbulence in order to achieve laminar flow conditions with a steady and uniform velocity distribution at the channel entrance. Airflow is passed through a 60 cm long entrance region and through a 60 cm test section and is then passed through a 30 cm long exit region. The air leaves through the outlet nozzle to the fan by a flexible hose. The flow velocity is measured using the air flow meter. The flow rate through the wind tunnel is measured with the velocity varying between 0.1 and 0.23 m/s. The flow meter gauge is calibrated using an orifice plate for several volume flow rates, and the least square method is applied to obtain the relation flow rate, as shown in Eq. (1). The temperature of the inlet air was measured by a thermocouple located at the entrance. The wind tunnel is mounted on a wooden board that allows the orientation of the wind tunnel to be changed for a range of longitudinal inclination angles (0°–70°) and a transverse lateral inclination in the range of (0°–90°).

$$Q_{ref} = -1912.6 \times Q_{exp}^3 + 88.201 \times Q_{exp}^2 - 0.5581 \times Q_{exp} + 0.0118 \quad (1)$$

where Q_{ref} is the standard flow rate, and Q_{exp} is the experimental flow rate.

2.2. The test section

The test section is a rectangular heated base with longitudinal fins. This section contains an aluminum plate that is 60 × 30 × 0.6 cm. The fin array is made from aluminum with 2 mm thick, 60 mm length. This array was installed on the aluminum plate by making 2 mm width grooves and 3 mm deep. The fins are embedded into the grooves of the aluminum base plate without clearance by pressing hard and forcing the fins into the grooves. The fins are then fixed by spot-welding along the aluminum plate, similar to how many studies embed longitudinal fins into the grooves of the base plate without welding [14,20,25]. The section view (A-A) in Fig. 1 of the rectangular duct is graphically displayed in Fig. 3 and shown photographically in Fig. 4. The insulated with 15 cm glass wool and a wooden box were implemented on all sides of the test section to insulate it from the ambient environment. Table 1 shows descriptions of the tested fin array.

2.3. Heater circuit

The test section bottom wall was constructed from a 6 mm aluminum plate heated with a heating element. A sheet heater was located under the aluminum plate, which was distributed along the aluminum plate, i.e., both have the same dimensions of 30 cm × 60 cm, as seen in Fig. 5.

The variation in the heater plate was provided by an electric current, providing the boundary condition of a constant heat flux for the experimental study. The plate was heated using an electrical heater, which consisted of a nickel-chrome wire that was wrapped up as parallel strips on an electrically isolated plate, but the heat-conductive was made of mica and covered by another mica plates (inserted between two mica sheets). The heater is situated in contact under of the base; the thickness of the heating element is equal to nearly 3 mm. The test section is completely insulated along all sides to drive all the heat to the fin array.

2.4. Thermocouple circuit

The base plate temperature was measured by a thermocouples set (type K NiCr-Ni) located inside an aluminum plate of thickness 6 mm. The thermocouples are installed in the bottom wall inside holes drilled in the aluminum plate, the diameter of drilling holes is 6 mm and the depth is 5 mm. The number of thermocouples was 24, which were

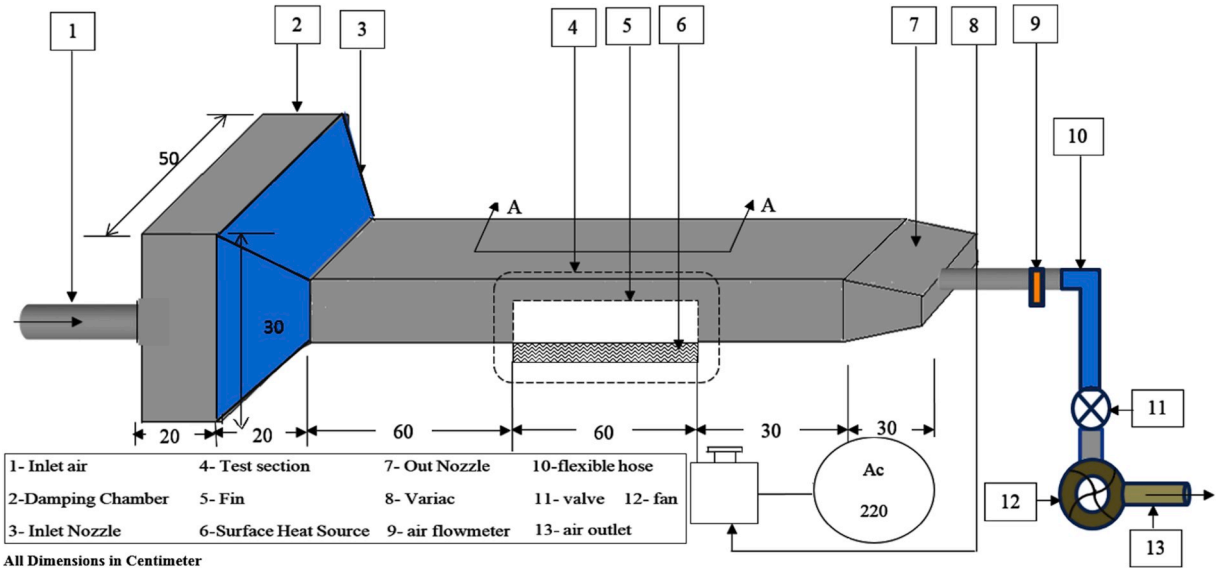

Fig. 1. Schematic diagram of the experimental setup.

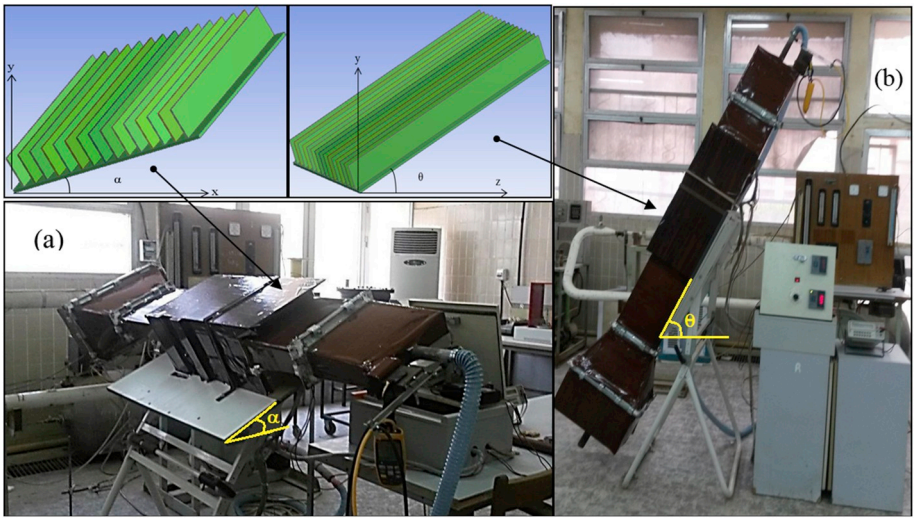

Fig. 2. Photo image of the experimental setup. (a) Lateral inclination case, (b) Longitudinal inclination case.

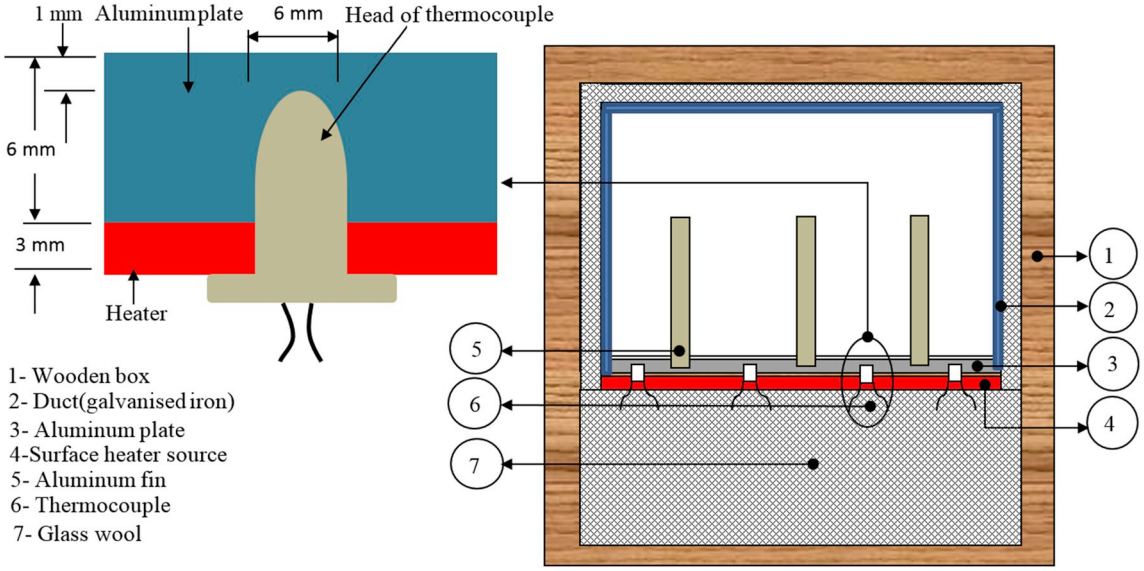

Fig. 3. Schematic diagram of the test section (section A-A).

distributed on the aluminum plate.

2.5. The experimental data

From the experimental study can be measured the voltage drop across the heater, temperature, electric current, and velocity. Then from the heated plate can calculate the average Nusselt number as follows:

$$Nu_{av} = \frac{h_{av} D_h}{k_{air}} \tag{2}$$

where h_{av}: the average heat transfer coefficient.

D_h: characteristic length.

k_{air}: thermal conductivity of air.

The average heat transfer coefficient expressed by Eq. (3) is frequently used in experimental studies and represented by the average surface temperature of the aluminum plate and air inlet temperature. The experimental verifications of Eq. (3), previously identified and adopted by many studies as an active method to determine the average heat transfer coefficient, are given in Refs. [14,20,25,26]. Furthermore, the channel hydraulic diameter D_h is known by Eq. (4).

$$h_{av} = \frac{Q_{convection}}{A_b (T_w - T_{in})} \tag{3}$$

$$D_h = \frac{4A_c}{P} \tag{4}$$

where A_b = L*W is the unfinned area of the heated wall, A_c is the duct cross-sectional area, $Q_{conv.}$ is the fluid convection heat transfer rate, T_w is the average heated wall temperature, P is the summation of edges of the duct and T_{in} is an air inlet temperature. The heat transfer from both the fins and heated aluminum plate by convection ($Q_{convection}$) is calculated by the energy balance [27–30], as follows:

$$Q_{total} = Q_{convection} + Q_{conduction} + Q_{radiation} \tag{5}$$

where Q_{total} is the total supplied power, $Q_{radiation}$ is the overall loss of radiation from the heated base and fin areas, and $Q_{conduction}$ is the overall heat loss from the isolation of the duct. Based on Ohm's law the overall energy provided to the heater can be calculated.

$$Q_{total} = V \times I \tag{6}$$

Heat loss was calculated in isolating the test section, as shown below:

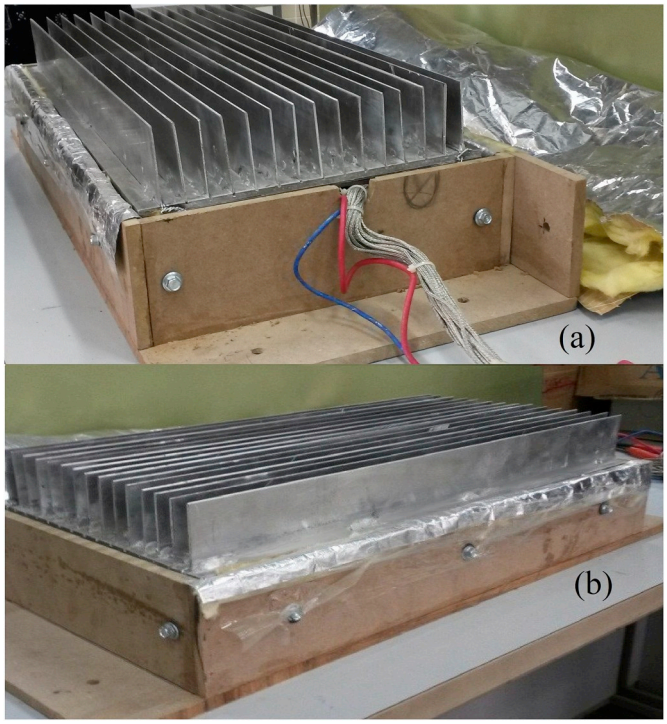

Fig. 4. Photo image of the test section (section A-A).

Table 1
Design considerations of the test fin array.

Parameter	Values
Thermal conductivity of fin, k_{fin}	237 W/m K
Duck width, W	30 cm
Duck height, H	10 cm
Fin number, N_{fin}	15
Fin length, L_{fin}	60 cm
Fin height, H_{fin}	6 cm
Fin thickness, t_{fin}	2 mm
Fin spacing, S	17 mm

$$Q_{coduction} = -k_{insulation} A_{insulation} \frac{\Delta T_{insulation}}{L_{insulation}} \tag{7}$$

where $k_{insulation}$ is the insulation for the thermal conductivity, $\Delta T_{insulation}$ is the inside and outside gradient temperature of the insulation.

Radiation losses are calculated from the following equation:

$$Q_{radiation} = F A_R \sigma (T_w^4 - T_b^4) \tag{8}$$

where F is the shape factor, A_R is the radiation surface area, and σ is the constant of Boltzmann, 5.67×10^{-8} W/m^2.K^4.

The Reynolds number:

$$\mathrm{Re} = \frac{w_{in} D_h}{\nu_{air}} \tag{9}$$

The Grashof number can be modified (Gr*) as:

$$Gr^* = \frac{g\beta \overline{\overline{q}}_{con} D_h^4}{k_{air} \nu_{air}^2} \tag{10}$$

where $\overline{\overline{q}}_{con} = \frac{Q_{convection}}{A_b}$ is the mean heat flux transported by convection to the air.

The properties of the fluid are calculated at an average of the heated plate and fluid inlet $\left(\frac{T_w + T_{in}}{2}\right)$.

3. Calibration of thermocouples

The accuracy of commercial measurement devices is less than the accuracy of equipped laboratory devices. To overcome this problem, a calibration process is carried out. The measured value found from a measuring tool is thus compared with the identified value of the test standard under definite reference conditions using measuring procedures.

The digital multimeter and its thermocouples were calibrated against the standard digital thermocouples for several readings. Using the least square method, the relation of the true temperature of the digital temperature gauge was performed and is as follows:

$$T_{ref} = 1.0778 T_{\exp} - 1.013 \tag{11}$$

where T_{ref} is the standard temperature, and T_{exp} is the experimental temperature.

The accuracy of the instruments applied to the case study is shown in Table 2.

4. Uncertainty analysis

To calculate the validity of the experimental study, a validation and uncertainty estimation (errors in measurements) is conducted on all measured quantities of heat supplied, thermocouple values, and fin array dimensions. According to Moffat's standard procedures [31,32], the uncertainties are estimated. Nusselt number uncertainty is approximately ± 5% and, for the modified Grashof number uncertainty, is approximately ± 3.5%. Reynolds number uncertainty is

Fig. 5. Photograph of the heater element.

Table 2
Measuring instrument list.

Mesured Paramter	Instrument	Range	Accuracy
Air temperature (Ta)	BES-01	-2-90 °C	± 0.5 °C
thermocouple	K NiCr-Ni	–	± 0.25%
multimeter	BS471110	–	± 1%
air velocity	Fluke 922	1–80 m/s	± 0.015 m/s
Airflow Meter	Fluke 922	0–99 m^3/hr	± 1%
wattmeter	BEEMET	0–2000 *w*	± 1%

approximately ± 3%. The average heat transfer coefficient uncertainty can be determined using Eq. (12) [33] and is approximately ± 1.74%.

Neglecting the conduction losses during the thin thermocouple wires because of the diameter less than 0.18 mm. Heat losses such as radiation, the thermal contact resistance of the fins, conduction losses during the isolation and conduction losses through the thin thermocouple are calculated in Appendix A based on Eq. (5). These losses were found to equal 12.07% to clarify that the maximum total heat losses do not exceed 13% of the overall power consumed [14,20,25]. The reduction in the total losses is mainly due to the fact that the duct is well insulated and that each fin was inserted by force into the groove and pushed down to make contact with the bottom of the groove in the base plate. Then fixed by spot-welding along aluminum plate beside, a molten 2024-T6 aluminum alloy (k = 185 W/m.K) was poured into an interface line between the fins and the bottom plate to reduce the thermal contact resistance, as shown in Fig. 4(b).

$$\frac{\Delta h}{h} = \sqrt{\left(\frac{\Delta Q}{Q}\right)^2 + \left(\frac{\Delta A}{A}\right)^2 + \left(\frac{\Delta(\Delta T)}{T}\right)^2} \tag{12}$$

5. Results and discussion

An experimental study for a rectangular fin array with the heat transfer of laminar mixed convection in a horizontal orientation with a longitudinal and lateral inclination of the rectangular duct, in which the lower wall is exposed to a uniform heat flux. Two different cases are investigated. In case one, measurements are performed for the lateral inclination angle, with a range α = 0°, 30°, 60°, and 90°. Case two is achieved by studying both the longitudinal and lateral inclination effects, with the lateral inclination angle varying from 0° to 90° and the longitudinal inclination range Θ = 0°, 30°, 60°, and 70°. The experiments were conducted under various flow conditions, ranging from Re = 1000 to 2300 and with a modified Grashof number $Gr^* = 3 \times 10^8$ to 1×10^9.

This paper seeks to test the more appropriate parameter to facilitate comparisons with other similar studies that adopted the average heat transfer coefficient h_{av} [14,20,25]. Thus, the coefficient of heat transfer has been considered the dependent variable. Furthermore, it is comparatively easier to calculate the coefficient of heat transfer than the Nusselt number. Accordingly, there are many studies that adopted the heat transfer coefficient as the dependent variable [34–37].

5.1. Case one: lateral inclination angles (α)

Fig. 6 illustrates the change of the local temperature of the heated surface along the distance extended from the inlet to the outlet of the test section for a lateral inclination angle α = 30°, Re = 2300 and several Grashof numbers. It clear from this figure that the temperature values in the entry of the test section have nearly the same inlet temperature and represent forced convection thermal conditions. Then, the temperature increases until it reached a maximum value of nearly z = 0.4 m. This result refers to the intensity of the buoyancy secondary flow. Furthermore, distribution of the local heat transfer coefficient for the lateral inclination angle α = 30° at Re = 2300 and the different modified Grashof numbers are shown in Fig. 6. In the entry zone of the test section, the forced convection features seem clear on the behavior of the heat transfer coefficient. After the short distance of the channel, instability begins in the buoyancy secondary flow, which prevents the continuance decline in the local heat transfer coefficient. This outcome due to the buoyancy strength, which becomes sufficient to instability the boundary layer.

Moreover, increasing in the heat transfer coefficient is distinguished. The mixed convection zone started after the secondary flow. The variations of the Grashof number on the coefficient of local heat transfer are presented in this figure. It can be seen that the heat transfer coefficient increases with the Grashof number.

The Grashof number's effect on the average convection heat coefficient distribution is shown in Fig. 7 for different Reynolds number and lateral inclination angles. For all lateral inclination angle cases, a remarkable change can be observed in the convection heat coefficient produced by an increase in the Grashof number. It is noticed that as Gr* increases above 3×10^8, a buoyancy-driven secondary flow adjacent to the heated walls develops, which quickly increases as Gr* continues to

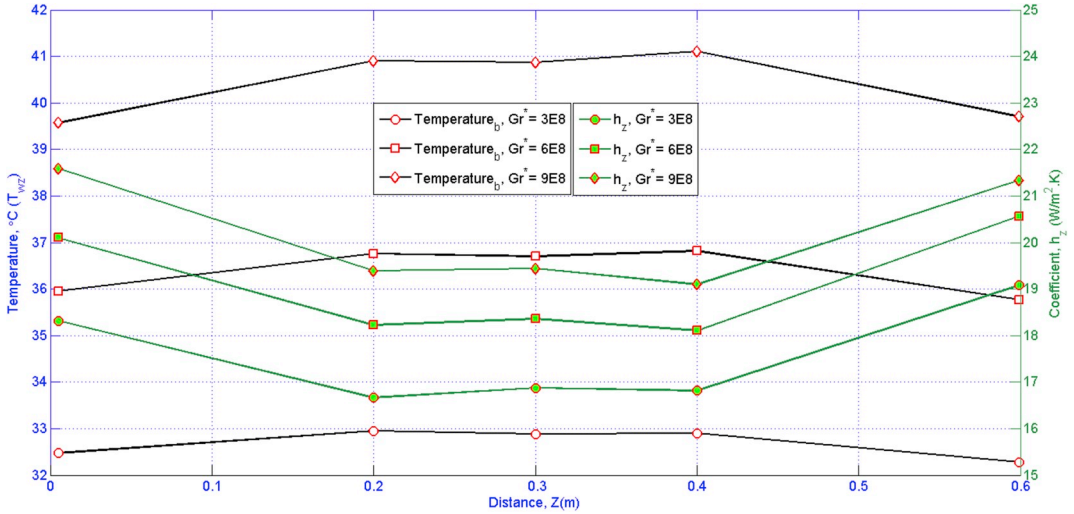

Fig. 6. Variation in the local base temperature and heat transfer coefficient for different Grashof numbers at angle α = 30°, Re = 2300.

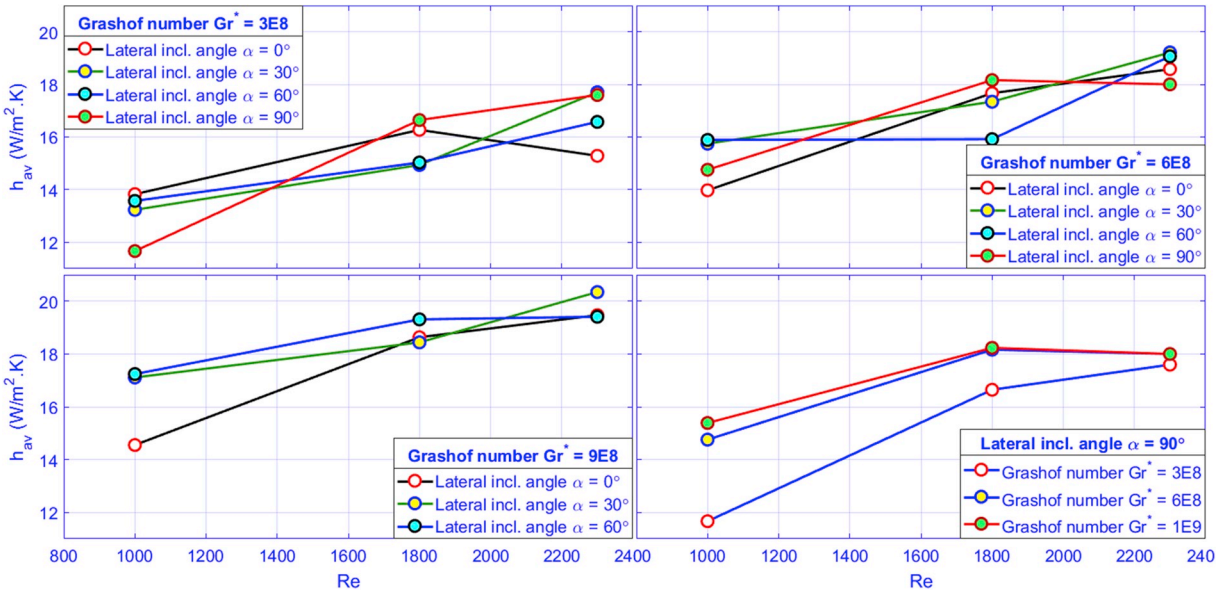

Fig. 7. Shows the change of average *h* with Reynolds number for several Grashof numbers and lateral inclination angles.

increase. The reason that a pressure gradient in the channel develops, which is against the inertial and buoyancy forces, is that it assists the secondary effect.

It is observed from this figure that the convection heat transfer coefficient with an orientation $\alpha = 60^{\circ}$, Re = 1000 and Re = 1800 is higher than other orientation angles when Grashof number $Gr^* = 9 \times 10^8$. Additionally, the convection heat transfer coefficient in the lateral inclination angle $\alpha = 30^{\circ}$ and Re = 2300 it has the maximum heat transfer rate at $Gr^* = 9 \times 10^8$. The low heat transfer process with a high orientation angle is due to the impeding air, which is generated by changing the angle so that the heated air that enters between the fins will hit the surface of the fins before leaving the sides.

The thickness of the thermal boundary layer increases with a reduction in Re. Because of this layer, heat transfer from the heated wall surface and the fin is decreased. There is a fluid flow entering the duct and passing through a channel between the fins. The heat exchanging takes place between the fresh air and the heated plate and goes out at the exit. As a result, h_{av} increases with increasing Re.

Fig. 8 Shows the change of the temperature in the heated wall T_{wz} and the local heat transfer coefficient h_z for lateral inclination angles $\alpha = 0^{\circ}$ and 90° at Re = 2300, respectively.

It is observed from Fig. 8 that the base temperature increases with an increasing Gr* and lateral inclination angle. With an increasing Gr*, the values of the surface temperature increase when the angle is changed from an upward orientation ($\alpha = 0^{\circ}$) to a sideways orientation ($\alpha = 90^{\circ}$). It is also clear from Fig. 8 that the coefficient of heat transfer diminishes as the heat sink is laterally inclined from the horizontal (upward orientation) $\alpha = 0^{\circ}$ to the vertical (sideways orientation) orientation $\alpha = 90^{\circ}$. For the orientation angle $\alpha = 90^{\circ}$, the fluid between the fin channels becomes hotter than the fluid above the tip fins. This

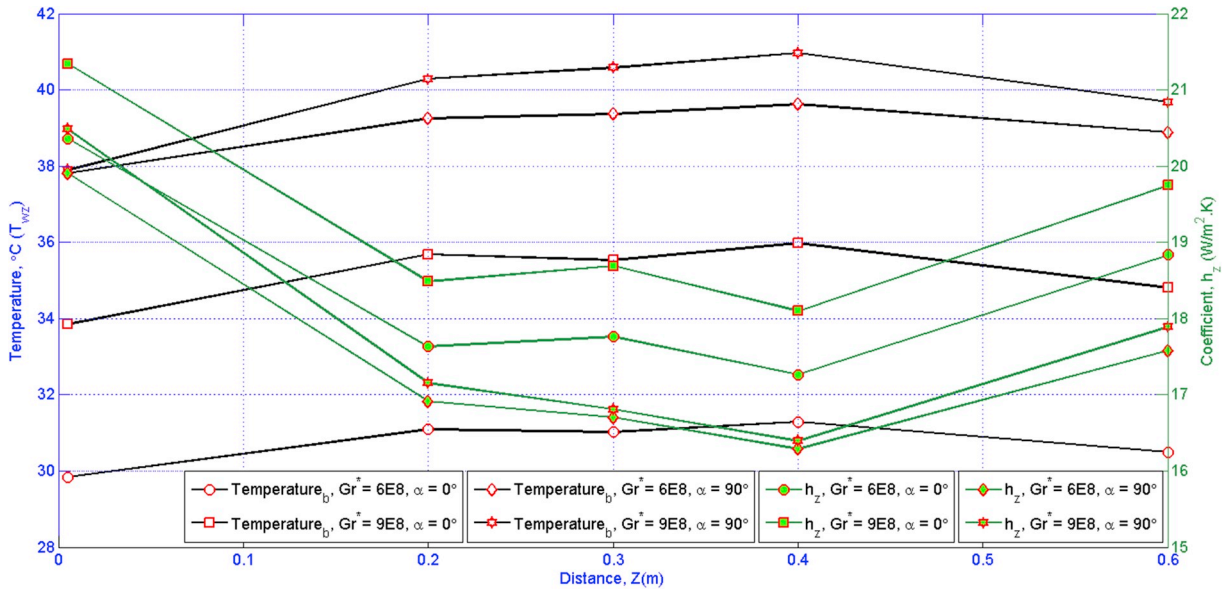

Fig. 8. Presented the local base temperature and *h* for different Gr* number and $\alpha = 0^{\circ}$, $\alpha = 90^{\circ}$ at Re = 2300.

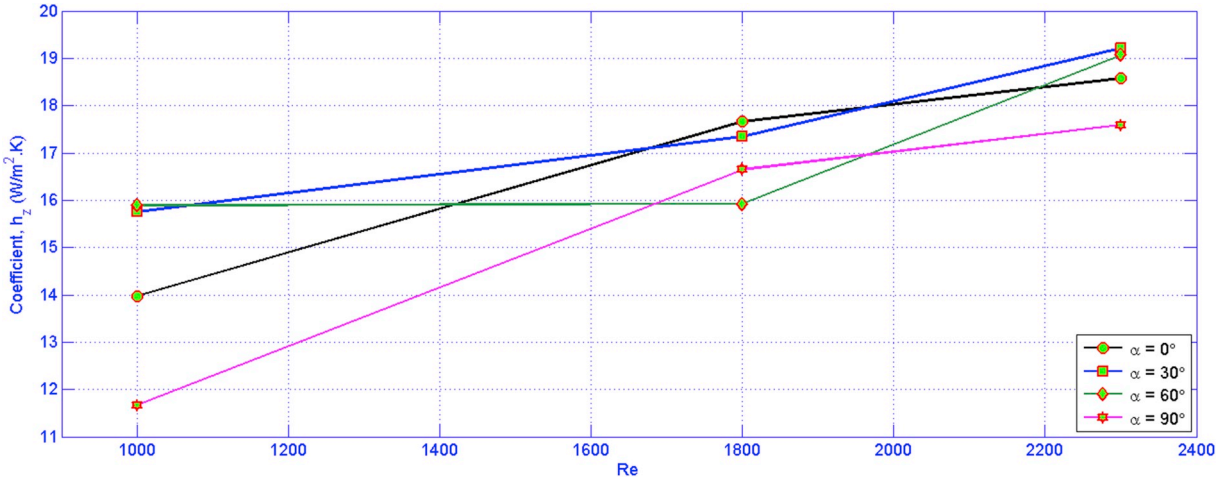

Fig. 9. Shows the change of average *h* with Reynolds number for lateral inclination angles α = 30°, α = 60°, and Gr* = 6 × 10^8.

outcome leads to a reduction in the coefficient of heat transfer.

It can be observed from this figure that the local heat transfer coefficient has the highest value at inlet due to a thin boundary layer and supremacy forced convection. Then, the coefficient of heat transfer is gradually decreased because there is a balance between the effect of all convection and buoyancy. Thus the buoyancy effect controls over the forced convection effect at the end part of the test section, leading to an increase in the local heat transfer rate.

Fig. 9 displays the variant of the average convection heat coefficient with regard to Re for lateral inclination angles α = 30°, α = 60°, and Gr* = 6 × 10^8. The orientation angle of fins α = 60° gives a coefficient of heat transfer less than that of α = 30° orientation. It is, therefore, concluded the rising heat transfer coefficient with decreasing α is due to the buoyant force produced by the change in air density when the temperature difference occurs. This outcome leads to more air entering between the fin channels for low values of α, which leads to an efficient heat exchange. Then air is heated in the course of the fin channels and goes up, while, with an increase in the lateral inclination angle, some of the hot air remains confined between the fins. Therefore, α = 30° orientation delivers the best performance for natural cooling.

Furthermore, the heat transfer coefficient is affected by the orientation as shown in Fig. 9 for different Reynolds numbers with lateral inclination angles α = 0° and α = 90° and Gr* = 6 × 10^8. The upward orientation (α = 0°) have higher values of heat transfer coefficient than that for the sideways orientation (α = 90°). The sideways orientation (α = 90°) causes the thermal boundary layer to concentrate on the fin surfaces. Therefore, there is a concentration of the boundary layers, resulting in a decrease in the fluid inflow velocity during fin arrays, avoiding the entry of fresh fluid into the fin channels. Therefore, the hot fluid remains longer among fin passages.

5.2. Case two: longitudinal inclination (Θ) and lateral inclination angle case (α = 90°)

This experiment was conducted to demonstrate the effect of both the longitudinal and lateral inclination angles on the heat transfer features of mixed convection laminar flow from fins inside a rectangular duct oriented with a lateral inclination angle α = 90° and longitudinal inclination ranges (Θ = 0°, 30°,60°,70°).

Fig. 10 shows the change of the local base temperature and

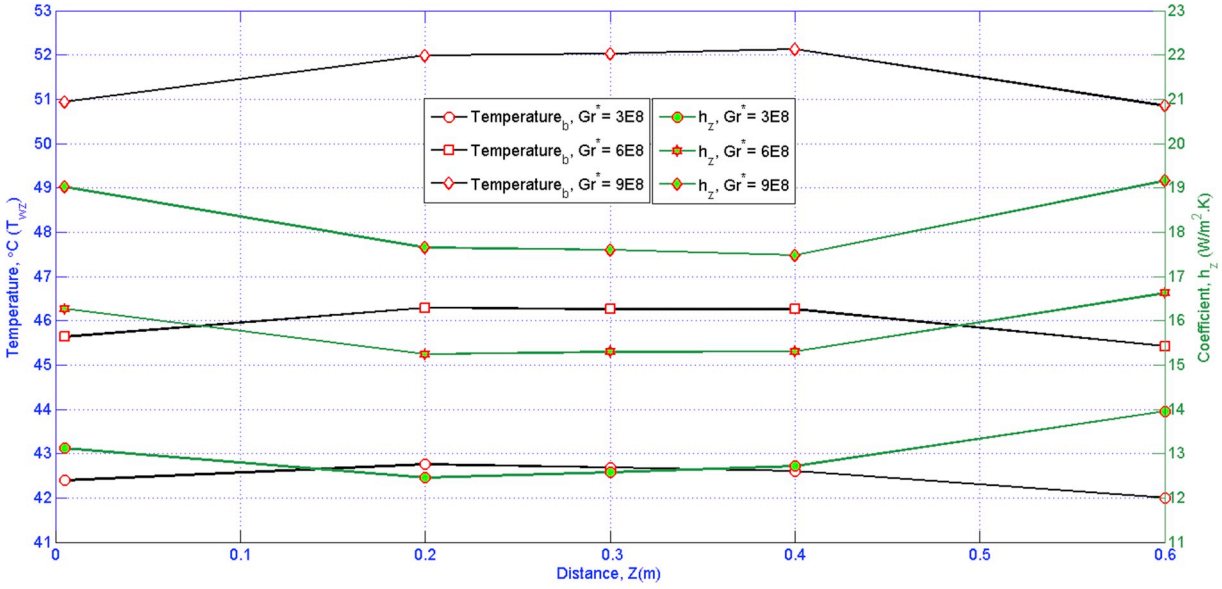

Fig. 10. Variation of local base temperature and convection heat coefficient for different Gr* at Θ = 60°, α = 90° and Re = 1000.

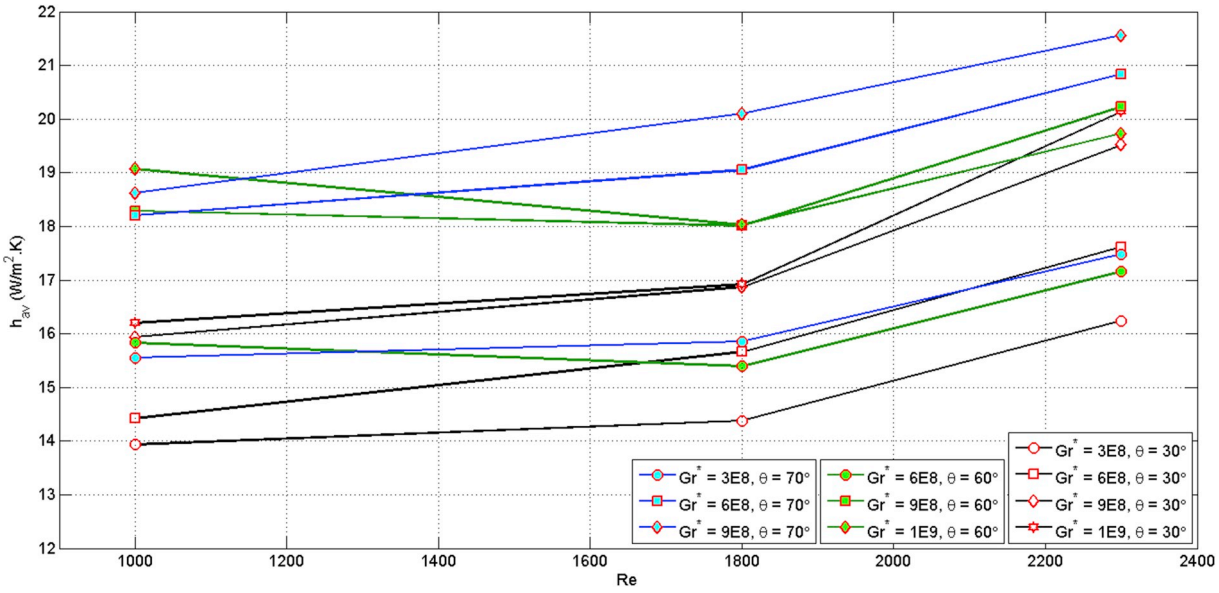

Fig. 11. Displays the convection heat coefficient with Re number for various Gr* number and Θ at α = 90.

coefficient of heat transfer for various Grashof numbers at longitudinal inclination angle Θ = 60°, Re = 1000, and a lateral inclination angle α = 90°. In the entrance part of the test section, the temperature is low and mostly, it is affected by the inlet temperature. Then, after some distance, the temperature increases because of the influence of mixed convection before decreasing from the mixing of hot and cold fluids.

At $Gr^* = 3 \times 10^8$, heat transfer occurs by conduction, which overcomes the convection mechanism. At $Gr^* = 6 \times 10^8$, the heat transfer mechanism through the duct is both forced convection and natural convection. As Gr* increases to 9×10^8, natural convection becomes the predominant heat transfer mechanism. It is detected that the base temperature rises with an increasing Gr*. As a result, the heat transfer coefficient increases, as can be noticed in Fig. 10.

To study the influence of the longitudinal inclination angle on the mechanisms of heat transfer for a horizontal and longitudinal inclined duct, in the heat transfer process exist three mechanisms that play an important role in heat transfer for the longitudinal inclined case. The convection is forced by these three mechanisms due to the uniform mainstream, where the direct free convection as a result of the component of the gravity vector parallel to the heated wall and the indirect free convection due to the component of the gravity vector normalized to the heated plate [38].

The effect of Gr* on the average heat transfer coefficient was studied in Fig. 11 for several Re and longitudinal inclination angles. The trend of the curves displays that the average heat transfer coefficient h_{av} rises with increasing Re and Gr* for all longitudinal inclination angles. In addition, the average heat transfer coefficient h_{av} rises with increasing longitudinal inclination angles Θ because the buoyant force is working in the flow direction, which will be improved with an increasing longitudinal inclination angle and the natural convection effect.

The average heat coefficient changes with the longitudinal inclination angle for different Reynolds numbers and $Gr^* = 6 \times 10^8$ and $Gr^* = 9 \times 10^8$ is shown in Fig. 12. From the figure, it is observed that

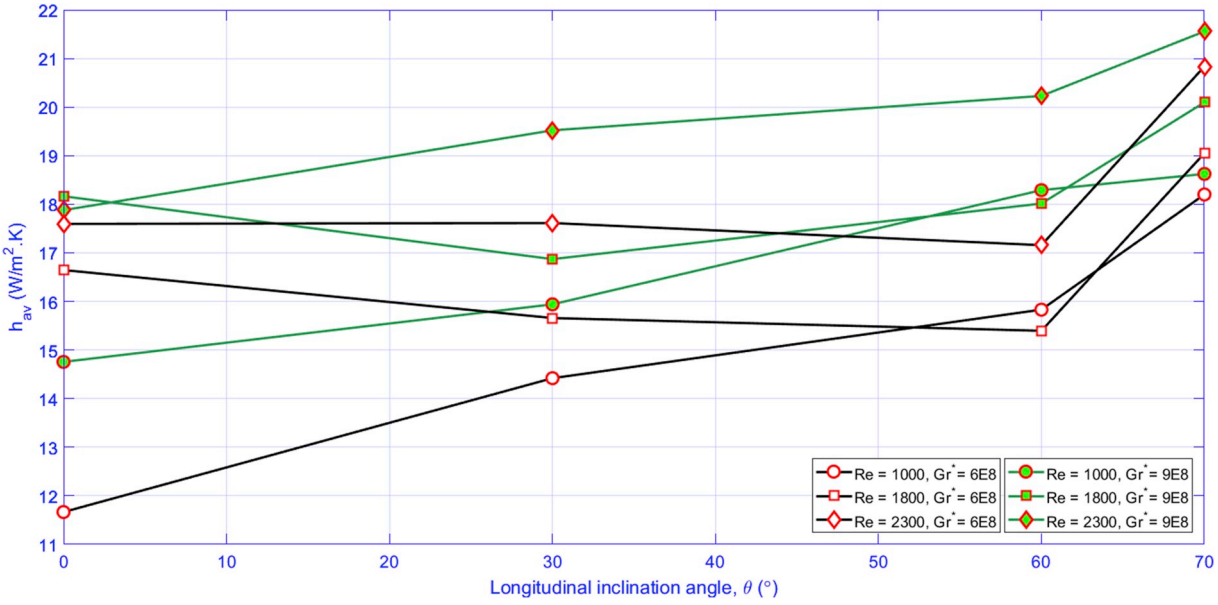

Fig. 12. Exhibits that the average of heat convection with Θ for several Re numbers and Gr numbers, with α = 90°.

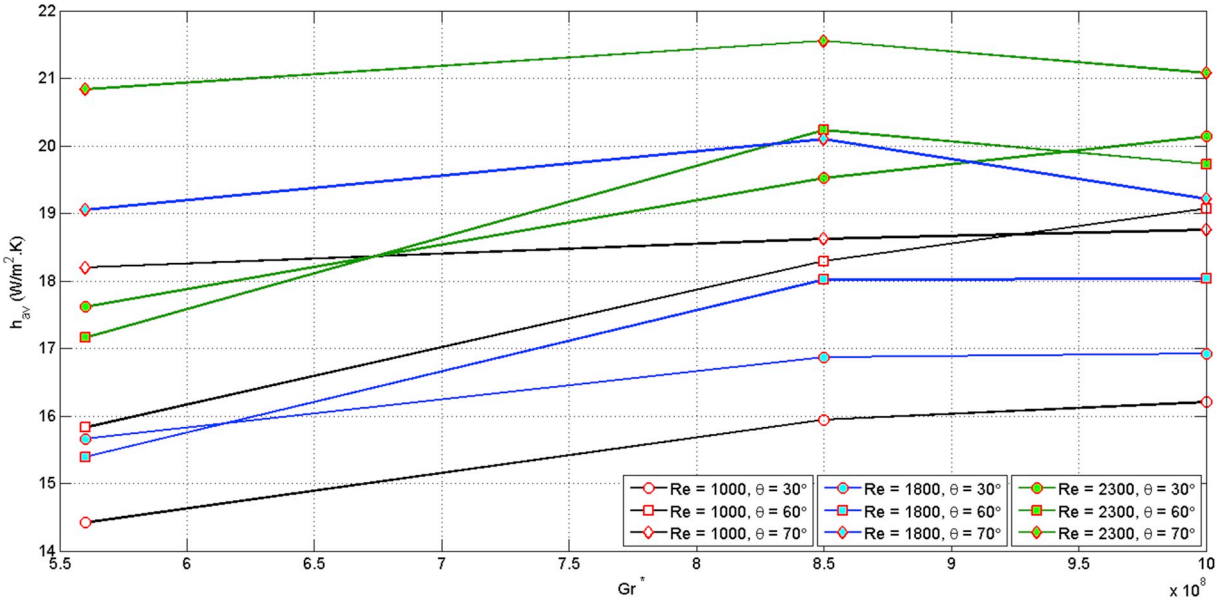

Fig. 13. Shows the change of the average heat coefficient with Gr* number for different Θ and Re numbers and α = 90°.

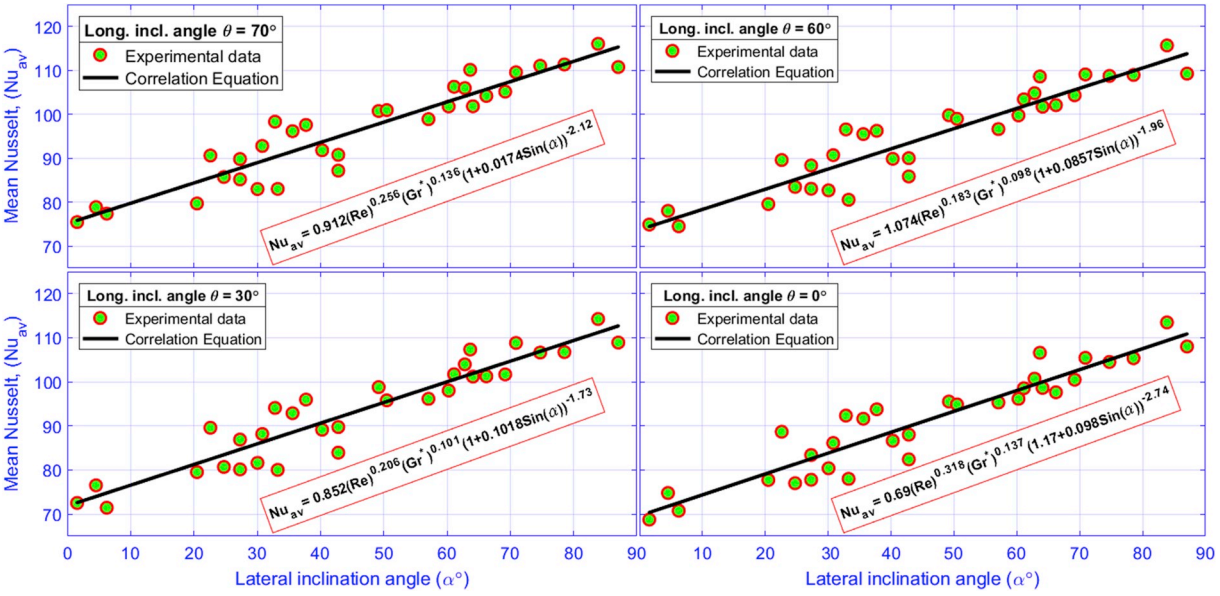

Fig. 14. Comparison of the correlation found from the data set and experimental consequences for lateral inclination angles.

$$Nu_{av} = (Re)^{0.256}(Gr*)^{0.136}0.912(1 + 0.0174\sin(\alpha))^{-2.12} \quad \text{for } \Theta=70^{\circ} \tag{13a}$$

$$Nu_{av} = (Re)^{0.183}(Gr*)^{0.098}\,1.074(1 + 0.0857\sin(\alpha))^{-1.96} \quad \text{for } \Theta=60^{\circ} \tag{13b}$$

$$Nu_{av} = (Re)^{0.206}(Gr*)^{0.101}\,0.852(1 + 0.1018\sin(\alpha))^{-1.73} \quad \text{for } \Theta=30^{\circ} \tag{13c}$$

$$Nu_{av} = (Re)^{0.318}(Gr*)^{0.137}\,0.69(1.17 + 0.098\sin(\alpha))^{-2.74} \quad \text{for } \Theta=0^{\circ} \tag{13d}$$

the coefficient of heat transfer increases as the longitudinal inclination angle rises. It is known that, as the longitudinal inclination angle varies from 0° to 70°, the strongest buoyancy force appears at higher longitudinal inclination angles (Θ > 0°) and the weakest at horizontal conditions (Θ = 0°).

For the lower longitudinal inclination angle of Θ = 30°, there are weak buoyancy forces, and fluid streams above the fin section prevent the hot fluid from escaping from the fin arrays. These phenomena lead to less in the performance of heat transfer. Additionally, for the higher longitudinal inclination angle Θ = 70°, the largest average heat transfer coefficient can be attained for all Re.

With increasing the Reynolds number, the velocity increases, which prevents the power of the secondary flow condition and decreases the development of the thermal boundary layer. A higher Re produces smaller variations in h_{av}. These features are noticed for Re = 2300, where secondary flow conditions are mostly absent, and the forced convection is the dominant mode.

Fig. 13 displays the change of the average heat transfer coefficient

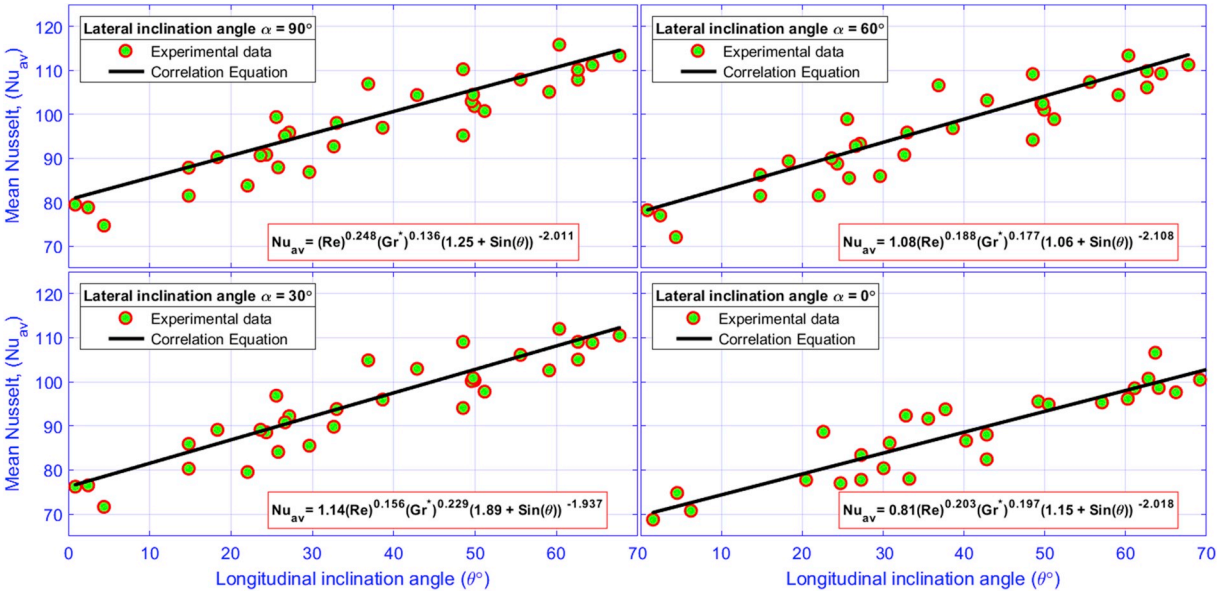

Fig. 15. The data set and experimental results for inclination angles are implemented to show a comparison of the correlation.

with various Gr* and Re. From this figure, for the longitudinal inclination angle Θ = 30°, a lower value of h_{av} is obtained. This result occurs because the effects of buoyancy, which are induced by natural convection, diminish, leading to in a low coefficient of heat transfer.

Furthermore, it is clear from this figure that the optimal angle for the desired heat transfer is while the longitudinal inclination angle Θ = 70°. This result is because of the body force component that accelerates the fluid because of it acts in the direction of axial flow, resulting from an increase in the heat transfer coefficient; this has an important role in the heat sink cooling. It can be deduced that the heat transfer coefficient increases when the fins are longitudinally inclined from a horizontal orientation. The fins orientation also plays a significant role in heat transfer enhancement.

5.3. Empirical correlations for the average Nusselt number

The variation of the heat transfer coefficient for the fins is due to the two tilting orientations that have been previously observed. This outcome gives a primary indicator as to how the Nusselt number will be changed based on how the two angles change. The empirical equations to correlate the mean Nusselt number are derived based on the Reynolds number, modified Grashof number, and the longitudinal and lateral inclination angles. Accordingly, the results are as expected, as shown in Fig. 14. Fig. 14 explains the empirical equations derived for the adoption of the lateral inclination angle as a dependent variable. The correlation can be written as follows:with the following ranges: $1000 \le Re \le 2300$, $3 \times 10^8 \le Gr^* \le 1 \times 10^9$ and $0^\circ \le \alpha \le 90^\circ$, a relative error of 9% and a correlation factor = 0.913.

Additionally, empirical equations are derived for case two (lateral inclination angles α and longitudinal inclination angle θ) to associate the average Nusselt number with the Reynolds number and modified Grashof number. Fig. 15 explains these equations. The correlation can be written as follows:

$$Nu_{av} = (Re)^{0.248}\,(Gr*)^{0.136}\,(1.25 + \sin(\theta))^{-2.011} \quad \text{for } \alpha=90^\circ \qquad (14a)$$

$$Nu_{av} = (Re)^{0.188}\,(Gr*)^{0.177}\,1.08(1.06 + \sin(\theta))^{-2.108} \quad \text{for } \alpha=60^\circ \qquad (14b)$$

$$Nu_{av} = (Re)^{0.156}\,(Gr*)^{0.229}\,1.14(1.89 + \sin(\theta))^{-1.937} \quad \text{for } \alpha=30^\circ \qquad (14c)$$

$$Nu_{av} = (Re)^{0.203}\,(Gr*)^{0.197}\,0.81(1.15 + \sin(\theta))^{-2.018} \quad \text{for } \alpha=0^\circ \qquad (14d)$$

with the following ranges: $1000 \le Re \le 2300$, $3 \times 10^8 \le Gr^* \le 1 \times 10^9$ and $0^\circ \le \theta \le 70^\circ$, $\alpha = 90^\circ$, a relative error not exceeding 9% and a correlation factor = 0.995.

6. Conclusions

Experimental studies were carried out for mixed convection heat transfer, laminar flow with fins inside a horizontal and inclined duct subjected to uniform heat flux at the bottom surface.

From the experimental study, the following can be concluded.

1 The results illustrate that the average heat transfer coefficient increased with Re and the Grashof number for all inclination angles.
2 Smaller fluctuations in h_{av} are observed with higher Re due to the absence of the secondary flow effects and the forced convection in the dominant mode.
3 A greater coefficient of heat transfer is observed at the highest longitudinal inclination angles.
4 The heat transfer coefficient decreases with an increasing lateral inclination angle.
5 As the longitudinal inclination angle increases, the buoyancy effect increases, which causes an unstable secondary flow and results in a fluctuation of the distribution of h_{av}.
6 From the experimental results, the equations of correlations are obtained to relate four main variables, independent variables (modified Grashof number, longitudinal and lateral inclination angles, and Reynolds number) and the dependent variable (the average Nusselt number) as shown in equations (13a)-(14d).

Appendix A

To prove the validity of the experimental system, its output result is compared with its input power, and the convection losses have been determined with good accuracy. The thermal balance equation can be expressed as follows [39].

$$Q = V*I \approx m*cp*(T_o - T_{in}) \qquad (1A)$$

where Q, V and I are the power, voltage and electric current for the heater circuit, respectively, m is the air mass flow rate, cp is the specific heat of the air, and T_o and T_{in} are the temperature at the outlet and inlet, respectively.

$$Q = A_c{*}\nu_m{*}\rho{*}cp{*}(T_o - T_{in}) \tag{2A}$$

where A_c is the cross-sectional area of the duct, ν_m is the mean velocity of the air, and ρ is the air density. cp and ρ are determined by the base temperature T_b.

$$T_b = \frac{\overline{T_\omega} + \overline{T_\alpha}}{2} = \frac{\overline{T_\omega} + T_o + T_{in}}{2} \tag{3A}$$

$$T_{in} = 28.3\,^{\circ}C,\ T_o = 35.4341\,^{\circ}C$$

$$\overline{T_\alpha} = \frac{T_o + T_{in}}{2} = 31.867\,^{\circ}C$$

$$T_b = \frac{\overline{T_\omega} + \overline{T_\alpha}}{2} = \frac{42.329 + 31.867}{2} = 37.098\ ^{\circ}C = 310.098 \approx 310K$$

$$Cp = 1.00546\ \frac{kJ}{kg.\ k} \text{ and } \rho = 1.1406\frac{kg}{m^3} \text{ at } T_b = 310K$$

$$\nu_m = 0.188\frac{m}{s}$$

$$Q = (0.1{*}0.3)m^2 * 0.188\frac{m}{s} * 1.00546 * 10^3\frac{j}{kg.\ k} * 1.1406\frac{k}{m^3} * (308.434 - 301.3)k$$

$$Q = 46.14348\ \frac{j}{s}$$

$$V{*}I = Q * A_b$$

$$\frac{220{*}0.226}{0.13} = \frac{49.68}{0.13} = \frac{46.14348}{loss}$$

$$loss = 0.1207$$

References

[1] R.Z. Homod, K.S.M. Sahari, Energy savings by smart utilization of mechanical and natural ventilation for hybrid residential building model in passive climate, Energy Build. 60 (2013) 310–329.

[2] R.Z. Homod, K.S.M. Sahari, H.A.F. Almurib, Energy saving by integrated control of natural ventilation and HVAC systems using model guide for comparison, Renew. Energy 71 (2014) (2014) 639–650.

[3] M.S. Ahmed, A. Mohamed, R.Z. Homod, H. Shareef, A.H. Sabry, K.B. Khalid, Smart plug prototype for monitoring electrical appliances in Home Energy Management System, Conference on Research and Development, 2015 IEEE, 2015, pp. 32–36.

[4] C.R. Kharangate, L.E. O'Neill, I. Mudawar, Effects of two-phase inlet quality, mass velocity, flow orientation, and heating perimeter on flow boiling in a rectangular channel: Part 2 – CHF experimental results and model, Int. J. Heat Mass Tran. 103 (2016) (2016) 1280–1296.

[5] Y. Yao, H. Wu, Z. Liu, A new prediction model for the effective thermal conductivity of high porosity open-cell metal foams, Int. J. Therm. Sci. 97 (2015) (2015) 56–67.

[6] R.Z. Homod, K.S.M. Sahari, H.A.F. Almurib, F.H. Nagi, Gradient auto-tuned Takagi-Sugeno fuzzy forward control of a HVAC system using predicted mean vote index, Energy Build. 49 (6) (2012) 254–267 2012.

[7] T.M. Liou, C.S. Wang, S.P. Chan, Effect of included angle on turbulent flow and heat transfer in rhombic serpentine heat exchangers, Int. J. Therm. Sci. 114 (2017) (2017) 155–171.

[8] S. Alfarawi, S.A. Abdel-Moneim, A. Bodalal, Experimental investigations of heat transfer enhancement from rectangular duct roughened by hybrid ribs, Int. J. Therm. Sci. 118 (2017) (2017) 123–138.

[9] M. Azzolin, S. Bortolin, D.D. Col, Flow boiling heat transfer of a zeotropic binary mixture of new refrigerants inside a single microchannel, Int. J. Therm. Sci. 110 (2016) (2016) 83–95.

[10] E.K. Lakhal, M. Hasnaoui, E. Bilgen, P. Vasseur, Natural convection in inclined rectangular enclosures with perfectly conducting fins attached on the heated wall, Int. J. Heat Mass Tran. 32 (1997) 365–373.

[11] J. Ma, F. Xu, Unsteady natural convection and heat transfer in a differentially heated cavity with a fin for high Rayleigh numbers, Appl. Therm. Eng. 99 (2016) (2016) 625–634.

[12] R.T. Huang, W.J. Sheu, Chi-Chuan Wang, Orientationeffect on natural convective performance of square pin fin heat sinks, Int. J. Heat Mass Tran. 51 (2008) 2368–2376 2008.

[13] Q. Qiu, X. Du, X. Zhu, Shengqiang Shen Study on flow and heat transfer in a finned internal cooling duct, Appl. Therm. Eng. 113 (2017) (2017) 58–69.

[14] M. Dogan, M. Sivrioglu, Experimental and numerical investigation of clearance gap effects on laminar mixed convection heat transfer from fin arrayin a horizontal channel-A conjugate analysis, Appl. Therm. Eng. 40 (2012) (2012) 102–113.

[15] S.M.J. Al-Azawi, Effect orientation on performance of longitudinal (trapezoidal) fins heat sink subjected to natural convection, AJES 2 (2) (2009).

[16] S.V. Naidu, V.D. Rao, B.G. Rao, A. Sombabu, B. Sreenivasulu, Natural convection heat transfer from fin arrays experimental and the theoretical study on effect of inclination of base on heat transfer, ARPN Journal of Engineering and Applied Sciences 5 (9) (2010) 7–15 2010.

[17] A.A. Walunj, D.D. Palande, Experimental analysis of inclined narrow plate-fins heat sink under natural convection, Int. J. Mech. Eng. 2 (6) (2014) 8–13 2014.

[18] H.E. Ahmed, Optimization of thermal design of ribbed flat-plate fin heat sink, Appl. Therm. Eng. 102 (2016) (2016) 1422–1432.

[19] J.R. Maughan, F.P. Incropera, Mixed convection heat transfer with longitudinal fins in a horizontal parallel plate channel: part II – experimental results", ASME J. Heat Transfer 112 (1990) (1990) 619–624.

[20] M. Dogan, M. Sivrioglu, Experimental investigation of mixed convection heat transfer from longitudinal fins in a horizontal rectangular channel, Int. J. Heat Mass Tran. 53 (9–10) (2010) 2149–2158.

[21] S.G. Taji, G.V. Parishwad, N.K. Sane, Enhanced performance of horizontal rectangular fin array heat sink using assisting mode of mixed convection", Int. J. Heat Mass Tran. 72 (2014) (2014) 250–259.

[22] M.H. Yang, R.H. Yeh, J.J. Hwang, Mixed convective cooling of a fin in a channel, Int. J. Heat Mass Tran. 53 (4) (2010) 760–771.

[23] B. Das, A. Giri, Mixed convective heat transfer from vertical fin array in the presence of vortex generator", Int. J. Heat Mass Tran. 82 (2015) (2015) 26–41.

[24] R.Z. Homod, Analysis and optimization of HVAC control systems based on energy and performance considerations for smart buildings, Renew. Energy 126 (2018) (2018) 49–64.

[25] M. Dogan, M. Sivrioglu, Experimental investigation of mixed convection heat transfer from longitudinal fins in a horizontal rectangular channel: in natural convection dominated flow regimes, Energy Convers. Manag. 50 (2009) (2009) 2513–2521.

[26] F.P. Incropera, D.P. Dewitt, T.L. Bergman, A.S. Lavine, Fundamentals of Heat and Mass Transfer, sixth ed., John Wiley & Sons, 978-0-471-45728-2, 2007.

[27] R.Z. Homod, Assessment regarding energy saving and decoupling for different AHU (air handling unit) and control strategies in the hot-humid climatic region of Iraq, Energy 74 (2014) (2014) 762–774.

[28] R.Z. Homod, K.S.M. Sahari, H.A.F. Almurib, F.H. Nagi, Double cooling coil model for non-linear HVAC system using RLF method, Energy Build. 43 (2011) (2011) 2043–2054.

[29] K.S.M. Sahari, M.F. Abdul Jalal, R.Z. Homod, Y.K. Eng, Dynamic indoor thermal comfort model identification based on neural computing PMV index" conference

series: earth and environmental science, IOP 16 (2013) (2013) 012113.
[30] R.Z. Homod, K.S.M. Sahari, H.A.F. Mohamed, F. Nagi, Modeling of Heat and Moisture Transfer in Building Using RLF Method, Conference on Research and Development, IEEE, 2010, pp. 287–292 2010.
[31] R.J. Moffat, Contributions to the theory of single-sample uncertainty analysis, J. Fluid Eng. 104 (1982) 250–260.
[32] R.J. Moffat, Using uncertainty analysis in the planning of an experiment, J. Fluid Eng. 107 (1985) 173–178.
[33] T.R. Taylor, An Introduction to Error Analysis—the Study of Uncertainties in Physical Measurements, University Science Books, Mill Valley, CA, 1980.
[34] U.V. Awasarmol, A.T. Pise, An experimental investigation of natural convection heat transfer enhancement from perforated rectangular fins array at different inclinations, Exp. Therm. Fluid Sci. 68 (2015) (2015) 145–154.
[35] T.K. Ibrahim, M.N. Mohammed, M.K. Mohammed, G. Najafi, N.A.C. Sidik, F. Basrawi, A. N Abdalla, S.S. Hoseini, Experimental study on the effect of perforations shapes on vertical heated fins performance under forced convection heat transfer, Int. J. Heat Mass Tran. 118 (2018) (2018) 832–846.
[36] E. Ayli, O. Bayer, S. Aradag, Experimental investigation and CFD analysis of rectangular profile FINS in a square channel for forced convection regimes, Int. J. Therm. Sci. 109 (2016) (2016) 279e290.
[37] M. Karami, M. Yaghoubi, A. Keyhani, Experimental study of natural convection from an array of square fins, Exp. Therm. Fluid Sci. 93 (2018) (2018) 409–418.
[38] C.C. Huang, T.F. Lin, Numerical simulation of transition aiding mixed convective air flow in a bottom heated inclined rectangular duct, Int. J. Heat Mass Tran. 39 (8) (1996) 1697–1710.
[39] R.Z. Homod, K.S.M. Sahari, H.A.F. Almurib, F.H. Nagi, RLF and TS fuzzy model identification of indoor thermal comfort based on PMV/PPD, Build. Environ. 49 (2012) (2012) 141–153.